High Power *X*-Band Monopulse Tracking Feed for the Lincoln Laboratory Long-Range Imaging Radar

KENNETH R. GOUDEY AND ATTILIO F. SCIAMBI, JR.

Abstract—**This paper covers the design, development, and test of a 10-GHz 10-percent bandwidth high-efficiency feed system to be used in a 120-ft Cassegrainian antenna for the M.I.T. Lincoln Laboratory Long Range Imaging Radar. The feed is a multimode monopulse tracking feed employing a multiflare horn and is capable of transmitting a power level of 800 kW at 50-percent duty. The feed will operate in both right- and left-hand circular polarization simultaneously or in both vertical and horizontal polarization simultaneously depending on the input network.**

INTRODUCTION

THE FEED required for the 120-ft diameter M.I.T. Long Range Imaging Radar antenna is shown in Fig. 1, where a single multimode horn is used in a Cassegrainian configuration to generate sum, azimuth, and elevation signals. The feed must be capable of transmitting very high power (800 kW with a 50-percent duty cycle at 10 GHz) and must exhibit very good amplitude and phase control of the radar signals over a 10-percent bandwidth. After installation in the Imaging radar, the feed will be used to transmit right-hand circular polarization and to receive both right- and left-hand circular polarization while tracking with either right- or left-hand circular polarization.

HORN DESIGN

In order to provide high efficiency and low off axis cross polarization when operating in circular polarization a feed horn with equalized *E*- and *H*-plane patterns and low spillover energy was required for the Long Range Imaging Radar. The first of three horn designs considered was the stepped input horn [1] which can generate the proper beamshape at a single frequency and fairly good beamshape over about a 5-percent bandwidth. However, due to the excessive length of the required horn over the 10-percent bandwidth, the degradation of the pattern at the band edges was too severe to consider this design. The second design was a corrugated horn [2] which has the desired pattern characteristics but has unknown performance at very high power. The corrugated horn design was rejected because of the risk of high-power arcing. The final design selected is the multiflare horn (Fig. 2) which has better bandwidth characteristics than the stepped horn and does not have the high-power handling risk of the corrugated horn.

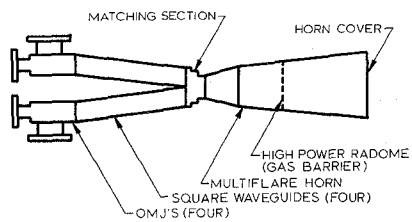

Fig. 1. Feed diagram.

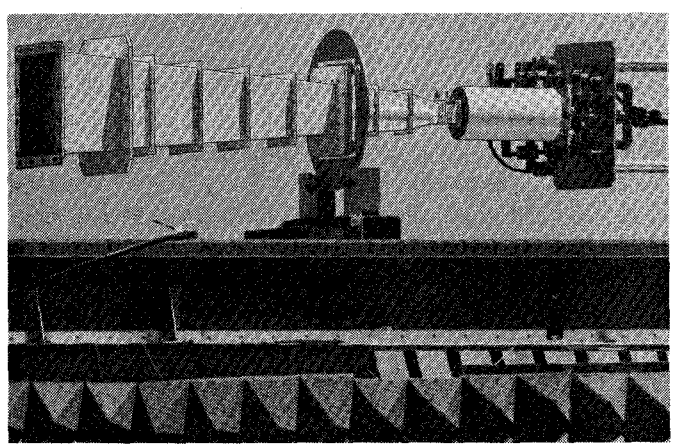

Fig. 2. Multiflare horn.

The better bandwidth characteristic of the multiflare horn is a direct result of the beamshaping mode being generated at a point where the horn has a large cross section, thereby minimizing differential phase shift. The development of a multiflare horn was based on the methods described by Cohn [3]. The approximate analysis given by Cohn was expanded upon and incorporated into a computer program for analysis of multiflare horns. A synthesis driver was then added to the computer program so that horn designs could be synthesized and an initial design for the feed was synthesized and built. This initial design was tested which pointed out errors in the analysis program which were corrected. Further iterations with the synthesis program brought out more problems in the analysis and methods to correct them were found. The final version of the synthesis program used to design the multiflare horn is quite accurate even out to the fourth

Manuscript received May 16, 1977; revised October 4, 1977.

The authors are with the Ford Aerospace and Communications Corporation, Western Development Laboratories Division, Palo Alto, CA 94303.

0018-9480/78/0500-0326$00.75

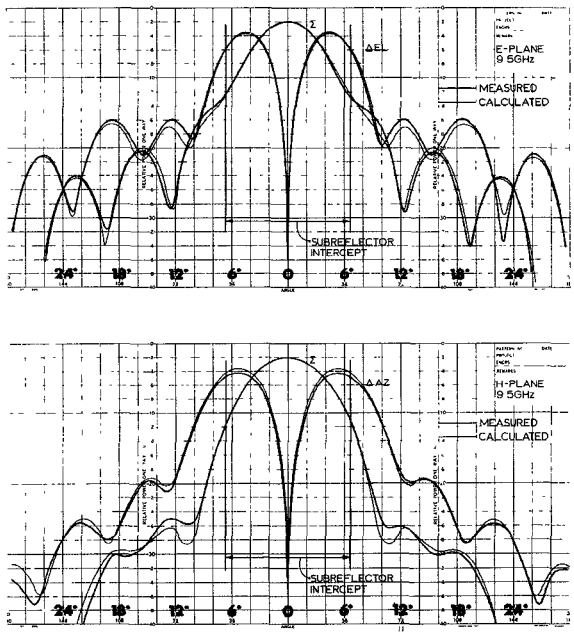

Fig. 3. 9.5-GHz measured and calculated radiation patterns (measured with a linearly polarized test horn).

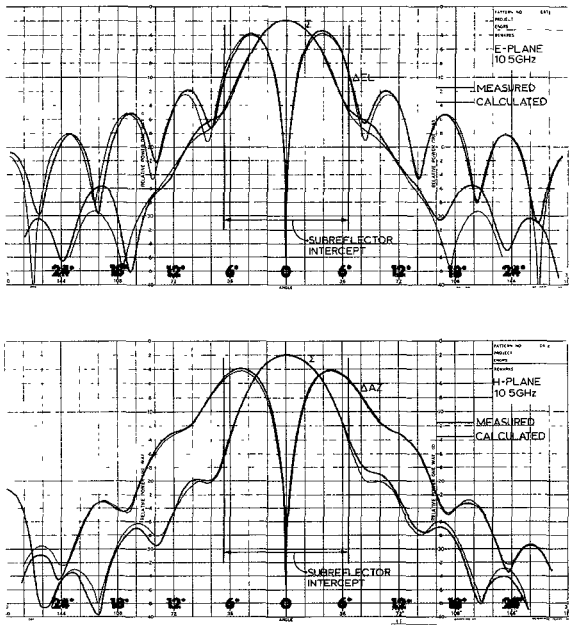

Fig. 4. 10.5-GHz measured and calculated radiation patterns (measured with a linearly polarized test horn).

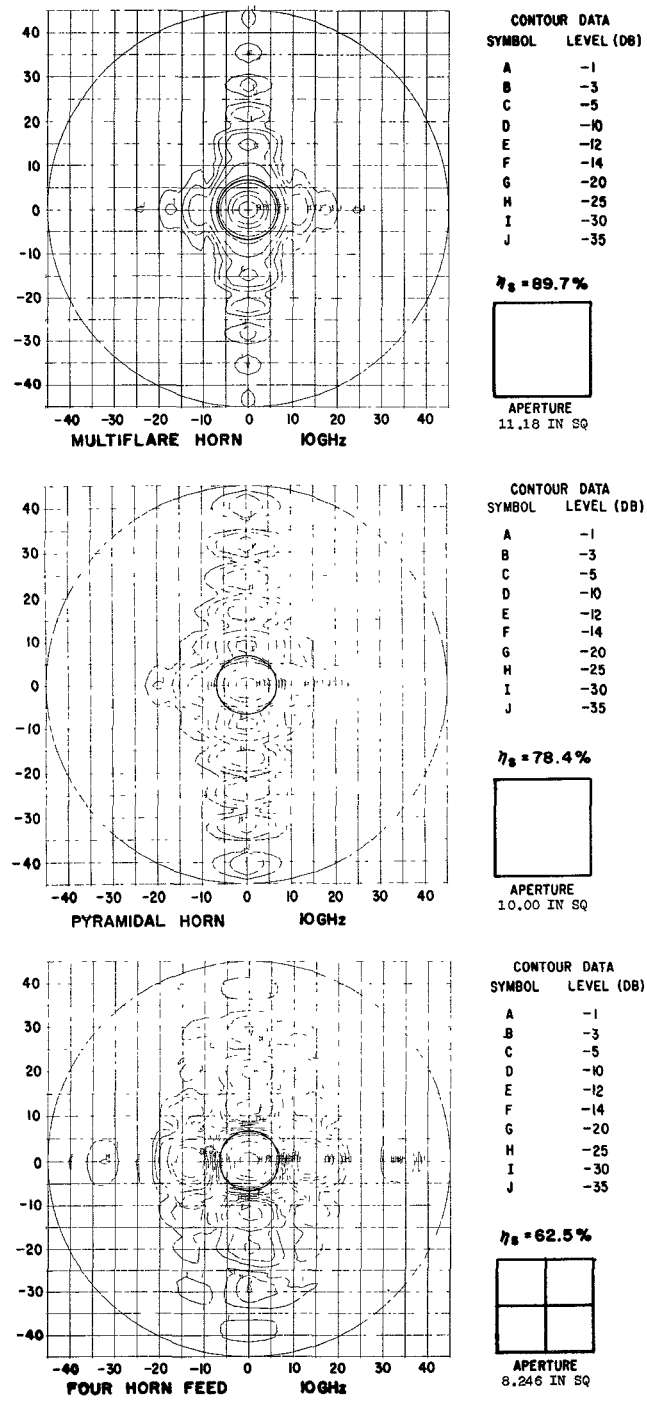

Fig. 5. Sidelobe energy comparison (linear polarization).

sidelobes of the horn radiation pattern. The final horn design was synthesized by the computer and built to the computed dimensions. This horn has measured radiation patterns which are nearly identical to the computed patterns. Figs. 3 and 4 are measured patterns of the final breadboard horn with the computed patterns superimposed in narrow lines. Both of these figures show the *E*- and *H*-plane sum patterns as well as the principal plane pattern for each difference channel, and illustrates the close agreement between measured and calculated radiation even out to the low-level sidelobes. During the synthesis of the multiflare horn two major goals were assigned to the computer program which attempted to synthesize the design of a horn meeting both of these goals. The first goal was low sidelobe (spillover) energy; the second goal was a circular beam over the subreflector intercept angle with a subreflector intercept level of 12 ± 2 dB between 9.5 and 10.5 GHz, and 12 ± 0.5 dB at 10.0 GHz. The total length of the horn was also constrained so that it would be consistent with the existing Cassegrainian geometry. The synthesis program could not successfully generate a horn design which fully satisfied both goals so a compromise became necessary in order to realize a design. The only goal which is not met in the final design is the intercept taper at the bottom of the band (9.5 GHz) which is approximately 9.5 dB in the *H* plane as can be

seen in Fig. 3. Figs. 3 and 4 illustrate that the other intercept levels fall within the goals. The achievement of low sidelobe energy is illustrated in Fig. 5 which shows a comparison between the contour patterns of the mutiflare horn, a four horn feed, and a simple pyramidal horn. The spillover efficiencies indicated on Fig. 5 as well as the contour maps themelves shows that the multiflare horn has lower spillover energy than either the square horn or the four horn feed. Fig. 5 also illustrates the beam circularity of the multiflare horn compared to a square horn. This beam circularity results from equalizing the *E*-, *H*-, and 45° plane patterns. The square horn has elliptical contours near the subreflector intercept angle whereas the multiflare horn has nearly circular contours. The four horn feed has nearly square contours near the subreflector intercept because its pattern shape depends heavily on the array factor of the four horns. It is also the array factor which makes the four horn feed spillover efficiency very low. The multiflare horn feed has both better beam circularity and higher spillover efficiency than either the square horn or the four horn feed.

Matching Section

In order to launch the sum and both tracking channels into a single horn, a multimode matching section was employed. The matching section consists of a junction between four square input waveguides and a single larger square output waveguide with an intervening square waveguide step transformer adjusted to match the TE_{10}, LSE_{11}, and TE_{20} modes into the horn when appropriate excitation is impressed on the four input waveguides. The following paragraph explains the matching methods used to launch all three modes without introducing tuning elements which might arc over at high power.

Referring to Fig. 6, the E_y electric field as a function of X at the input junction has double half-sine distribution while the desired distribution is a single half-sine. This results in reflected TE_{10} mode from the input junction, as well as propagated TE_{10}, and a number of evanescent modes which cannot propagate. A step (step 1 in Fig. 6) is introduced to generate reflected TE_{10} mode to cancel the TE_{10} reflected mode from the input junction. However, because this step must step in both dimensions to accommodate both vertical and horizontal polarization, undesirable LSE_{12} mode is generated with an amplitude $A_{12}E_{10}$ (Fig. 6) which will extract power from the TE_{10} mode. Therefore, a second step (step 2 in Fig. 6) is introduced to effect cancellation of undesirable LSE_{12} mode. With the two steps introduced, LSE_{12} mode cannot exist between steps 1 and 2, so step 1 generates LSE_{12} which is reflected at the input junction and cancelled when it returns to step 1. This means step 1 is adjusted so that LSE_{12} mode is not actually generated in the matching section. Step 1 also reflects some TE_{10} mode which partially cancels the reflected TE_{10} at the input junction. Step 2 is then adjusted to cancel the remaining reflected TE_{10} mode at the input junction.

The next step is to match the LSE_{11} mode. Since the LSE_{11} mode is transverse to X with respect to its electric field, it has an E_z component which cannot be launched directly off the 4 waveguide junctions. Therefore, there is a tendency to launch an excess of TE_{11} mode and to mismatch at the junction. In order to generate nearly pure LSE_{11} mode, probes are introduced at the input junction as shown in Fig. 6. Unlike the TE_{10} mode which can generate LSE_{12} mode in the matching section, the LSE_{11} mode cannot generate any higher order propagating modes in the matching section, which means the steps act like a simple transformer. The transformer steps for the LSE_{11} mode are fairly well matched when the TE_{10} mode has been matched. However, slight adjustment of the steps is necessary for best LSE_{11} match. The TE_{20} mode has a natural match at the input junction and, like the LSE_{11} mode the steps act as simple transformers because no higher order propagating modes are launched. The TE_{20} mode does not match thru the steps very well when they are adjusted for the TE_{10} or LSE_{11} mode. Therefore, eight ridges are added on the peaks of the TE_{20} mode electric field as shown in Fig. 6. When the LSE_{11} mode and the TE_{20} mode have been adjusted for best match, it is necessary to go back and readjust the match of the TE_{10} mode which is somewhat affected by the addition of the probes and ridges. Finally, all three modes are adjusted for the best compromise match to complete the matching section design.

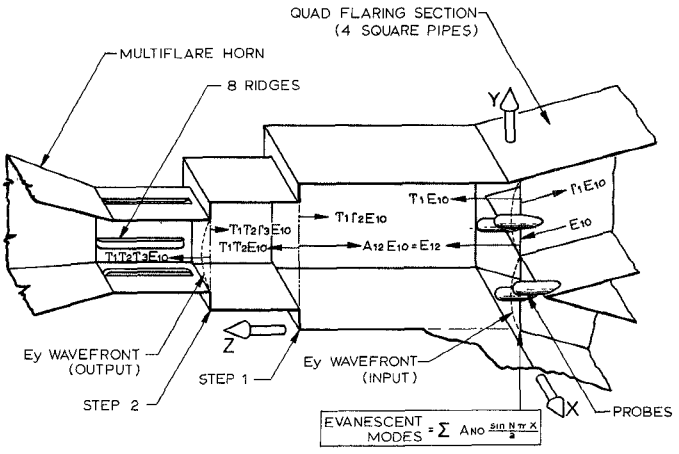

Fig. 6. Cutaway view of matching section.

Orthomode Junction

Each of the four square input waveguides to the matching section is fed by an orthomode junction (OMJ) so that either vertical or horizontal polarization may be launched into each square waveguide. The OMJ's also provide circular polarization by using quadrature excitation of both ports of each OMJ. In order to satisfy the overall system performance an OMJ was required which would have low VSWR, flat phase characteristics, and high isolation between ports. Existing OMJ designs were examined and characteristics were found in these designs which prevented achieving both good VSWR and flat phase. Basically each of these designs had orthogonal arms which, although cut off to each other, were not sufficiently cut off which led to a VSWR characteristic that had to be matched with a number of inductive or

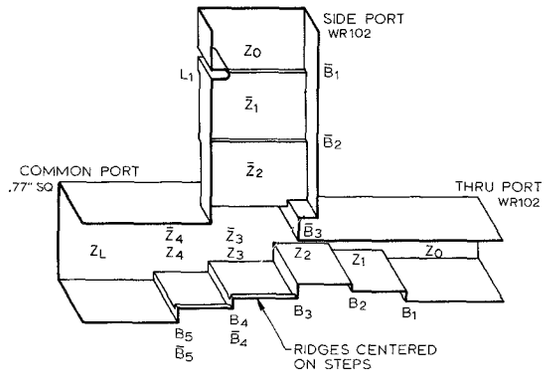

Fig. 7. OMJ impedance diagram.

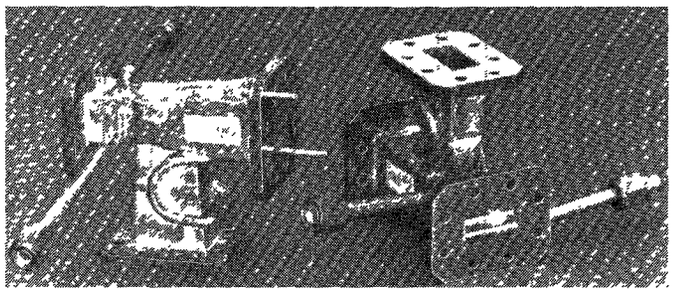

Fig. 8. High-power test OMJ's.

capacitive elements. This in turn yielded a nonflat phase characteristic and low isolation. In order to overcome the above difficulties a new approach was used in the design of the OMJ. Fig. 7 shows an impedance diagram of the OMJ design. The section labeled Z_2 is a reduced height guide section in order to provide a well cut off guide as seen by the side port. Similarly the section labeled $\bar{Z}_2$ is also reduced height to provide a well cut off section as seen by the thru port. Each arm of the OMJ is a four section maximally flat transformer in order to provide a good impedance match. There are small ridges on the bottom of the Z_3 and Z_4 sections in order to adjust the $\bar{Z}_3$ and $\bar{Z}_4$ impedances relative to the Z_3 and Z_4 impedances. These ridges make the transformer sections for the thru arm into ridge loaded waveguide sections, however, for the side arm the ridges are virtually not seen since they are perpendicular to the electric field. The lengths of the various sections in the thru arm were adjusted to match out the reactances B_1 thru B_5. At this point there are not a sufficient number of degrees of freedom to match out all of the reactances $\bar{B}_1$ thru $\bar{B}_5$ so an inductor L_1 was added to complete the side port matching.

The OMJ was designed for high power by rounding all protruding interior corners and adding water cooling tubes to carry away the heat generated by I^2R losses. In addition the height of various cross sections were not allowed to be so small that arcing might occur and finally tuning elements which might arc were avoided (e.g., capacitive buttons).

After the design was complete, two high-power test versions of the OMJ (shown in Fig. 8) were electroformed and taken to M.I.T. Lincoln Laboratory for high-power tests in a resonant ring on October 8, 1974. The OMJ's handled a power level of 100-kW CW in the side arm and

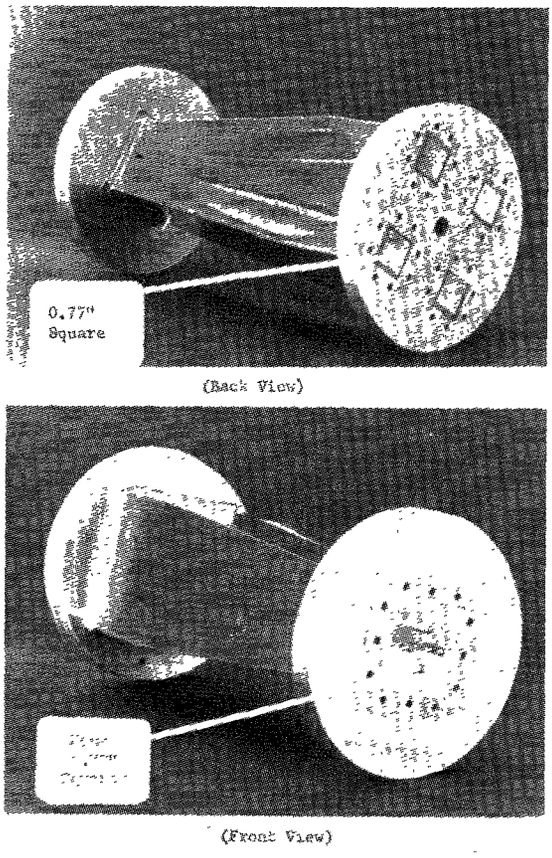

Fig. 9. Quad flaring section (outer wall of water jacket removed).

125-kW CW in the thru arm in a dry air/nitrogen atmosphere. This means that these OMJ's can safely handle the required 100-kW pulse at 50-percent duty when the system is pressurized with SF_6 or Freon 116.

Comparator

In order to impress the necessary excitation at the inputs of the four OMJ's to launch the sum and both tracking channels in each polarization, two orthogonal test comparators were constructed. One comparator is used for vertical polarization and the other comparator is used for horizontal polarization. These comparators may be seen at the far right side of Fig. 2, attached to the feed.

Cooling

The requirements for very high power necessitate that all of the feed components be adequately cooled. In order to provide this cooling, all of the feed components are made of electroformed copper with copper tubes attached to the outside of the walls for water cooling. The four square waveguides which go from the OMJ's to the matching section (quad flaring section) are encased in a water bath to provide adequate cooling where four waveguides come together as shown in Fig. 9. The smaller section of the multiflare horn below a 5-in cross section is also water cooled. The large section of the horn where the wall currents are much smaller is fabricated of aluminum and is not water-cooled in order to reduce the weight of the feed.

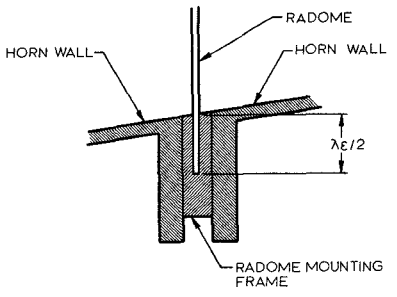

Fig. 10. Radome mounting frame.

Feed Radome

In order to pressurize the feed system with SF_6 or Freon 116 it was required that a radome be incorporated in the feed horn capable of withstanding 2 lb/in^2 differential pressure and passing the full transmitter power. In order to provide such a radome it was necessary to examine the various potential radome materials to find one strong enough to stand the pressure and low enough loss to pass 400-kW CW at 10 GHz. First a list of low loss materials was compiled and their strength properties examined. This resulted in a reduced list of candidates which were mechanically and RF power tested. Those candidates which looked most promising from calculated results were poly-imide film, polytetrafluoroethylene film (PTFE), PTFE-E glass cloth laminate, and PTFE-quartz glass cloth laminate. A test vessel was constructed which has a volume sufficient so that if small volumes of gas escaped a pressure change could be detected. One end of this vessel was fitted with a removable cover. A window frame of like size and design to that of the feed radome was fitted into this cover. Thus one side of the window was exposed to the ambient pressure and gas while the closed side was exposed to controlled pressure and gas compound. Several materials and bonding techniques were evaluated under various conditions of pressure, temperature, and gas compounds. The final selection of materials was a PTFE-quartz cloth laminate 12 mils thick bonded to the aluminum frame.

In order to mount the radome into the horn without danger of series arcing at the horn wall the mounting frame shown in Fig. 10 was designed. This frame has a slot to clamp the radome material which was designed to be a half wavelength long. The half-wavelength slot reflects the short at the bottom of the slot back to the horn wall and therefore makes the wall electrically continuous. The choke had to be $\lambda/2$ in the dielectric medium of dielectric constant ϵ_r. The value of ϵ_r for the PFTE-quartz laminate as published by the manufacturer was 2.47. In order to verify this value a sample of the material was sent to M.I.T. Lincoln Laboratory for measurement and a sample was measured at Ford Aerospace. The M.I.T. Lincoln Laboratory measurements indicated a value for ϵ_r of 2.35 and a loss tangent of 0.00052. The lower value measured may have been due to the fact that a stack of pieces was used for the measurement and that it was virtually impossible to squeeze all of the air out of the stack. A waveguide measurement of a single layer of the material was conducted at Ford Aerospace and the measured value of ϵ_r was 2.44 which is very close to the published value of 2.47. Therefore, the 2.47 value was used for the choke design.

Feed Efficiency

The overall efficiency of a Cassegrainian antenna system may be broken down into a number of component parts some of which are associated with the feed system and some of which are independent of the feed system. In order to evaluate the performance of the feed for the M.I.T. Lincoln Laboratories Long Range Imaging Radar a feed efficiency is defined and then a comparison between the multiflare horn feed efficiency and four horn feed efficiency is made. Feed efficiency is defined to consist of factors which are feed dependent only and may be written as

$$\eta_F = \eta_L \eta_S \eta_a \eta_p \eta_x$$

where

- η_F feed efficiency
- η_L feed loss efficiency
- η_S spillover efficiency
- η_a aperture illumination efficiency
- η_p phase efficiency
- η_x cross polarization efficiency.

The feed efficiency may be calculated by making microwave measurements of the feed loss and radiation patterns and using a computer integration program to integrate the radiation patterns and calculate all of the component parts of the feed efficiency. In order to calculate accurate values of η_S wide angle feed patterns must be measured at a large number of azimuthal angles and a very large number of data points must be entered into the computer. An alternate method of computing η_F has been derived by Ruze [4] which requires much less input data for the computer. This method basically substitutes a feed gain measurement for the integration of η_S. The first step in using this method is to redefine η_F as

$$\eta_F = \eta_I \eta_a \eta_p$$

where $\eta_I = \eta_L \eta_S \eta_x$ is the aperture intercept efficiency which means it is the ratio of the energy intercepted by the aperture in the proper polarization to the input power of the feed. The expression for η_I may be rewritten as

$$\eta_I = \frac{\int_0^{2\pi} \int_0^{\theta_r} P(\theta,\phi) \sin\theta \, d\theta \, d\phi}{\int_0^{2\pi} \int_0^{\pi} P(\theta,\phi) \sin\theta \, d\theta \, d\phi} \eta_L \eta_x$$

where θ_r is the intercept angle and $P(\theta,\phi)$ is the normalized power pattern of the feed. Feed gain is given by

$$G_F = \frac{4\pi}{\int_0^{2\pi} \int_0^{\pi} P(\theta,\phi) \sin\theta \, d\theta \, d\phi} \eta_L \eta_x$$

which may be substituted into the equation for η_I to

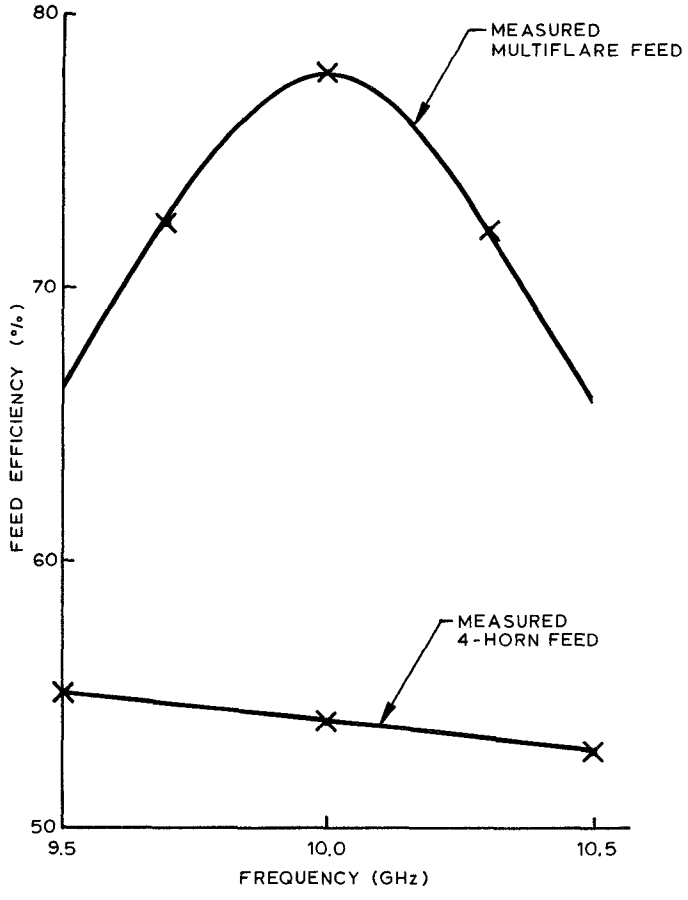

Fig. 11. Feed efficiency.

eliminate the wide-angle integral. The resulting equation is

$$\eta_I = \frac{G_F}{4\pi} \int_0^{2\pi} \int_0^{\theta r} P(\theta,\phi) \sin\theta \, d\theta \, d\phi$$

where the feed gain G_F is obtained from a range measurement of the feed gain and all three efficiencies involved in calculating η_F involve integrations over the aperture intercept angle only. Since the feed pattern is a relatively smooth function over the aperture intercept angles a limited number of input data points is sufficient to define the radiation pattern in this region. A computer program was used to calculate the normalized integrated power over the intercept angle region. The integrated power (P_I) as printed out by the computer program is given by

$$P_I = \frac{1}{2\pi} \int_0^{2\pi} \int_0^{\theta r} P(\theta,\phi) \sin\theta \, d\theta \, d\phi.$$

We may therefore rewrite the feed efficiency equation as

$$\eta_F = \frac{G_F P_I}{2} \eta_a \eta_p$$

where G_F is obtained from a feed gain measurement and P_I, η_a, and η_p are obtained by using the computer program to integrate patterns over the intercept angles only.

Efficiencies were calculated for both a four horn feed and the multiflare feed from measured patterns, and the results are plotted in Fig. 11. The efficiency of the multiflare feed exceeds the efficiency of the four horn feed by

TABLE I
EFFICIENCY SUMMARY

Multiflare Horn				
Frequency (GHz)	$(\%)\eta_I$	$(\%)\eta_a$	$(\%)\eta_p$	$(\%)\eta_F$
9.7	83.0	88.5	98.3	72.2
10.0	91.7	86.6	98.1	77.9
10.3	87.7	84.4	97.3	72.0
Four Horn Feed				
Frequency (GHz)	$(\%)\eta_I$	$(\%)\eta_a$	$(\%)\eta_p$	$(\%)\eta_F$
9.5	61.8	88.9	99.5	54.7
10.0	62.5	86.7	99.7	54.0
10.5	63.0	83.5	99.4	52.3

24 percent at 10.0 GHz and by at least 10 percent over the remainder of the band. Table I gives a breakdown of the efficiencies for both the multiflare feed and the four horn feed. From this table it can be seen that the primary disadvantage of the four horn feed lies in its low intercept efficiency.

CONCLUSIONS

A high-power high-efficiency single-aperture tracking feed was developed for the M.I.T. Lincoln Laboratory Long Range Imaging Radar. This feed is capable of transmitting a power level of 800 kW at 50-percent duty. In order to achieve high-feed efficiency a computer program was written to synthesize multiflare horns for beam shaping. The final horn design was built exactly to the computed dimensions and the performance realized was almost identical to the computed performance. The final feed had a feed efficiency of 78 percent at 10.0 GHz and at least 65 percent over the remainder of the operating band. The feed also had equalized *E*-, *H*-, and 45° plane patterns which resulted in a circular beam and low off axis cross polarization for the radar system. Tracking was accomplished in the feed by the use of the LSE_{11} and TE_{20} modes. A matching section was developed to match four square waveguides into one larger square waveguide before entering the horn so that the data and tracking modes could both be launched. This matching section was also designed to handle the high transmit power. Circular polarization was also a requirement of this program. In order to launch circular polarization into each of the four square waveguides entering the matching section, OMJ's were used so that the orthogonal input ports could be fed in quadrature. The OMJ's were also designed for high power. Tests at M.I.T. Lincoln Laboratory revealed that the OMJ's were capable of handling 100-kW CW in each port. A high-power radome was also developed for use at a five inch square cross section in the horn so that the feed could be pressurized to two psi with a gas such as SF_6. This radome material is capable of withstanding 25 kW/in^2. The M.I.T. Lincoln Laboratories Long Range Imaging Radar uses pulse compression which dictates gain and phase flatness over the 1-GHz bandwidth. All of

the feed components were designed to achieve both flat gain and phase across the operating band. Measured amplitude response of the final feed showed a gain ripple of less than 0.3 dB and a phase ripple of less than ±2° across the entire 9.5- to 10.5-GHz operating band.

ACKNOWLEDGMENT

The authors wish to extend their thanks to C. Jones, Dr. J. Ruze, W. Fitzgerald, and H. Kusinoki for their invaluable assistance in the course of the development of this feed.

REFERENCES

[1] P. D. Potter, "A new horn antenna with supressed sidelobes and equal beamwidths," *Microwave J.*, pp. 71–78, June 1963.
[2] D. Davis, "Corrugations improve monopulse feed horns," *Microwaves*, pp. 58–63, Apr. 1972.
[3] S. B. Cohn, "Flare angle changes in a horn as a means of pattern control," *Microwave J.*, pp. 41–46, Oct. 1970.
[4] J. Ruze, *Radar Astronomy*. New York: McGraw-Hill, 1968, pp. 411–420.

A Mode Transducing Antenna

ROBERT D. WENGENROTH, MEMBER, IEEE

Abstract—**At power levels above those readily handled by standard waveguide, and for long waveguide runs, the TE_{01} mode in circular guide is a preferred transmission line approach. At the antenna, this mode is generally unsuited to radiation since it forms a conical, instead of a pencil beam. Phase and polarization shifting techniques at a reflecting surface cause the illumination to be transduced to form a pencil beam. The techniques have been demonstrated in a 33-GHz model.**

I. INTRODUCTION

AN ANTENNA radiating a pencil beam when fed from a circular waveguide operating in the TE_{01} mode is a desirable component for extremely high power systems. Such an antenna has been demonstrated.

The TE_{01} mode in circular waveguide has several desirable features. It is a low-loss mode. It has a large cross section which permits it to guide high total power at moderate power densities. Wall currents are circumferential; longitudinal contact is not required in waveguide section joints. As a result, rotary joints are simple. Mode conversion tends to be low for the usual discontinuities associated with tolerances in the guide and in the assembly. All modes except the TE_{0n} are readily absorbed, thus avoiding coherent energy transfer into other modes by repeated discontinuities. A new class of extremely high power generators, the "gyrotron" or "cyclotron-master" [1], operates in the TE_{01} mode, increasing the interest in this mode.

In the antenna, a circular TE_{01} mode has a fundamental limitation; it is circularly symmetrical and radiates a conical beam with a null on axis rather than a pencil beam [2]. The fields must be converted to those which produce an acceptable pencil beam, either before the antenna or in the antenna. This is accomplished in the mode transducing antenna, in any of its several configurations; an input TE_{01} mode is transformed to radiate a pencil beam with either a circular or a linear polarization. Monopulse operation is feasible with a mode-separating feed assembly. Applications of the mode-transducing antenna all feature low-loss lines to handle extreme power levels. Examples are millimeter wave radars (search or track), satellite communications earth stations, and millimeter wave point-to-point communications.

Manuscript received June 13, 1977; revised October 15, 1977.
The author is with the Electronics Systems Division, General Electric Company, Syracuse, NY 13221.

II. THE MODE TRANSDUCING ANTENNA

The basis of the mode transducing antenna is the adjustment of the phase and polarization of the wave in the aperture by a modified reflecting surface in the antenna. The approach could also be implemented in transmission through a lens. If a TE_{01} mode were radiated from a circular aperture and the far zone field were probed with a linearly polarized receiver, the three and 6-dB contours for one linear component of the field would appear as shown in Fig. 1. The orthogonal linear polarization contours are identical to those shown, but rotated 90° mechanically about the center of the aperture. These components are in phase. Circular polarization is available by phase correction only, while linear polarization requires a twist-reflector [3] for efficient implementation. The reflection surfaces can be at the folds in folded circular horns, the main reflector in a single-reflector antenna, or the subreflector in a Cassegrain-type or other multiple reflector antenna.

III. MODEL TESTS

Three practical configurations of mode transducing antenna were demonstrated at 33.5 GHz in a folded conical horn antenna as shown in Fig. 2. The basic folded horn was described in 1963 [4] and a different application of

0018-9480/78/0500-0332$00.75